Experimental Behavior of One-Way RC Ultra-Thin Slabs Retrofitted with Post-Installed NSM CFRP Rods

Alaa N.A. Al-Nussairi[1] and Ahmed S.H. Suwaed[1,*]

[1]*Department of Reconstruction and Projects, University of Baghdad, Baghdad, Iraq*

Abstract: This study evaluates the flexural behavior of ultra-thin (50 mm) one-way reinforced-concrete (RC) slabs retrofitted with near-surface mounted (NSM) carbon-fiber-reinforced polymer (CFRP) rods under quasi-static loading. T300-grade CFRP rods (≈4 mm diameter) were bonded in pre-cut 7 mm × 7 mm grooves using a two-part epoxy. As a proof-of-concept experimental baseline, three simply-supported specimens (1000 mm × 500 mm × 50 mm) were tested in a six-point bending configuration (four applied loads + two reactions): two conventional controls and one strengthened slab. A load-control rate of ~15 kN/min was applied; the controls were cycled twice and the strengthened slab four times. Relative to the average of the two control specimens, the strengthened slab achieved ~+103% ultimate load (49.4 kN vs 24.3 kN) with a ~24% reduction in ductility (μΔ = 2.4 vs 3.15). Hysteretic dissipation, computed as loop area per cycle, was markedly higher for the strengthened slab; cycle-matched comparisons (cycles 1–2) are reported alongside cumulative values. The results show that NSM CFRP can markedly enhance capacity and energy absorption of very thin one-way slabs, with a trade-off in ductility that should be considered in design.

Keywords: Ultra-thin slabs, Near-surface mounted CFRP rods, Energy dissipation, Structural retrofitting, Concrete strengthening.

1. INTRODUCTION

Thin reinforced-concrete (RC) slabs can reduce self-weight and material use, allowing smaller columns and foundations and faster construction. The trade-off is tighter serviceability and shear limits: thin members are more susceptible to excessive deflection, cracking, flexure–shear interaction, and— in two-way systems—punching. Changes in use, increased imposed loads, or durability degradation often necessitate strengthening.

Near-surface mounted (NSM) carbon-fiber-reinforced polymer (CFRP) reinforcement is a practical retrofit for flexural strengthening of RC members. By placing CFRP rods/bars (or strips) in shallow grooves and bonding them with epoxy, NSM offers improved anchorage and bond relative to externally bonded reinforcement (EBR), better protection from mechanical damage, and minimal impact on member depth and clearance. However, its performance in very thin slabs is not well documented: limited cover constrains groove size and edge distance; epoxy shear and cover splitting can govern; and premature local debonding can limit gains.

Over the past two decades, CFRP systems have been widely adopted to retrofit RC members—including slabs, beams and columns—under both quasi-static and high-rate (impact/blast) demands. Applications span externally bonded (EBR) fabrics/strips and NSM rods/bars. Numerous EBR studies report gains in ultimate load and ductility of RC elements (*e.g.*, Frangou *et al*., 1995; Silva & Lu, 2007; Berger *et al*., 2008; Razaqpur *et al*., 2009; Wang & Wang, 2013; Azevedo *et al*., 2024). Other retrofit strategies include autoclaved multi-ply CFRP laminates for interior columns and walls (Muszyński & Purcell, 2003); hybrid systems combining EBR CFRP with polyurea coatings (Kim *et al*., 2009; Ha *et al*., 2011); and FRP strip strengthening of two-way slabs at low loading rates (Mosallam & Mosalam, 2003; Tabatabaei *et al*., 2012). Despite this breadth of EBR work, evidence on NSM CFRP rods in very thin slabs remains limited—particularly regarding bond, cover-splitting and edge-distance effects—motivating the present study.

NSM strengthening was first reported in Scandinavia in the 1940s, where steel rebars were installed in narrow grooves cut into existing concrete and grouted (Asplund, 1949). Durability was limited by steel corrosion (Alkhrdaji & Nanni, 1999). Replacing steel with fiber-reinforced-polymer (FRP) bars bonded with epoxy largely eliminates corrosion concerns and improves durability. Compared with EBR, which leaves CFRP exposed and more sensitive to environmental actions and mechanical damage, NSM places the CFRP within the cover, reducing exposure and improving anchorage (David & Neuner, 2001).

Experimental work on NSM CFRP spans multiple member types. Barros *et al*. (2006) and Wu *et al*. (2007) reported quasi-static tests on RC beams and columns strengthened with NSM CFRP rods/bars. Täljsten *et al*. (2003) examined cement-based grout as the groove adhesive. Hosseini *et al*. (2014) applied

*Address correspondence to this author at the Department of Reconstruction and Projects, University of Baghdad, Baghdad, Iraq;
E-mail: ahmed.shakir@uobaghdad.edu.iq

Received on 16-09-2025 Accepted on 20-10-2025 Published on 22-10-2025

E-ISSN: 2311-8717/25

prestressed NSM CFRP laminates/strips to RC slabs. A comprehensive treatment of NSM mechanics, bond, and detailing is provided by De Lorenzis & Teng (2007). Aljidda *et al*. (2023) investigated the use of NSM-GFRP bars for strengthening corrosion-damaged RC slabs, while Sharaky *et al*. (2023) examined one-way concrete slabs strengthened with NSM-CFRP rods; however, their specimens were of normal thickness (120 mm), and the strengthening was applied only to the tension face.

In contrast, the present study focuses on ultra-thin (50 mm) slabs strengthened on both faces, representing a configuration that has not been previously reported. Most research on NSM systems has concentrated on reinforced concrete (RC) beams, while thin one-way slabs (~50 mm) remain underreported. Because these slabs typically lack shear reinforcement, their small effective depth limits concrete shear strength—particularly near the supports—and flexural strengthening can shift the governing failure mode to one-way shear. The small thickness also prevents the use of two steel layers (no compression reinforcement), resulting in a shallow compression zone and increasing the likelihood of top-face crushing. These constraints justify dedicated experimental testing of NSM CFRP systems in thin one-way slabs.

Objectives: (i) quantify changes in ultimate load and stiffness; (ii) evaluate energy dissipation under cyclic loading; (iii) assess ductility; and (iv) document failure modes and bond behavior specific to thin-section detailing. Findings are reported relative to companion controls to enable reproducible benchmarking.

2. EXPERIMENTAL PROGRAM

2.1. Specimens

Three one-way RC slab specimens were cast to assess the effect of NSM CFRP on thin sections under quasi-static loading. All slabs measured 1000 × 500 × 50 mm and were simply supported in the tests. Two specimens served as controls (no CFRP); one specimen was strengthened using NSM CFRP on both faces.

Flexural steel (tension) was identical in all slabs: a single bottom layer of 7Ø6 mm ribbed bars placed in the span direction. The steel area was $A_s = 7 \times (\pi \cdot 6^2/4) = 197.9$ mm², giving a steel ratio $\rho s = A_s/(b \cdot t) \approx 0.0079$ (0.78%), with b = 500 mm and t = 50 mm. Distribution steel and cover details are reported in §2.2.2/§2.3.2.

The strengthened slab received NSM CFRP rods installed in pre-cut 7 mm × 7 mm grooves and bonded with a two-part epoxy: seven Ø4 mm rods at the bottom (tension) face and three Ø4 mm rods at the top (compression) face (T300 grade). Rod spacing, edge distances, groove layout and bonded length are shown in Figure **1**. All other materials were identical. Table **1** summarizes specimen IDs and reinforcement layouts.

Choice of steel ratio: ρ_s was selected to achieve (i) adequate tension-steel ductility and (ii) peak loads within the 100 kN capacity of the available instrumentation. Minimum reinforcement was checked per EC2 (EN 1992-1-1) using $A_{s,min} = 0.26\ fctm/f_{yk} \cdot b \cdot t \geq 0.0013\ b\ t$; no blanket “4% maximum” per EC2 is claimed here.

Table 1: Specimen Details and CFRP Layout

Specimen	Type	f'c (MPa)	CFRP – Top (compression)	CFRP – Bottom (tension)
QC1	Control	28	—	—
QC2	Control	35	—	—
QS1	Strengthened	43	7Ø4 mm	3Ø4 mm

Table 2: Concrete mix per ~50 L batch

Item	Quantity	Notes
Cement (CEM I 32.5R)	16.5 kg	1.00 part (by mass)
Fine aggregate (sand)	25.0 kg	1.52 parts
Coarse aggregate (10 mm)	50.0 kg	3.03 parts
Water	4.75 L (≈4.75 kg)	w/c ≈ 0.29
Accelerator	0.40 L	≈2.4% bwoc
Plasticizer	50 mL	≈0.3% bwoc

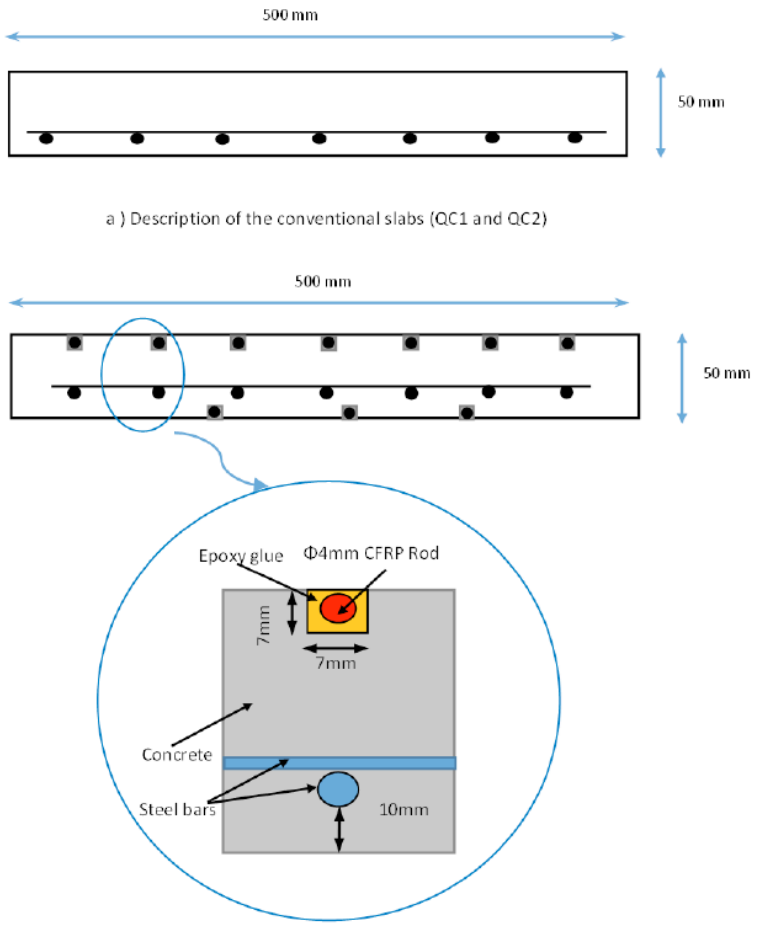

Figure 1: Contrasts Between (**a**) Conventional and (**b**) Strengthened Slabs

2.2. Material Properties

2.2.1. Concrete

Concrete was produced with CEM I 32.5R, fine aggregate (sharp sand), and coarse aggregate (10 mm gravel/crushed limestone). Materials were batched by mass and mixed in a 50 L mixer in multiple batches. The target water–cement ratio was w/c ≈ 0.29 by mass (4.75 kg water per 16.5 kg cement). An accelerator and a plasticizer were added to improve early-age strength and workability. The per-batch mix is given in Table **2**.

Companion 150 mm cubes were made for each specimen. Two were tested in 7 days and two on the day of slab testing. Compressive strength testing followed BS EN 12390-3:2019; specimen

Figure 2: Concrete compressive test of the cubes.

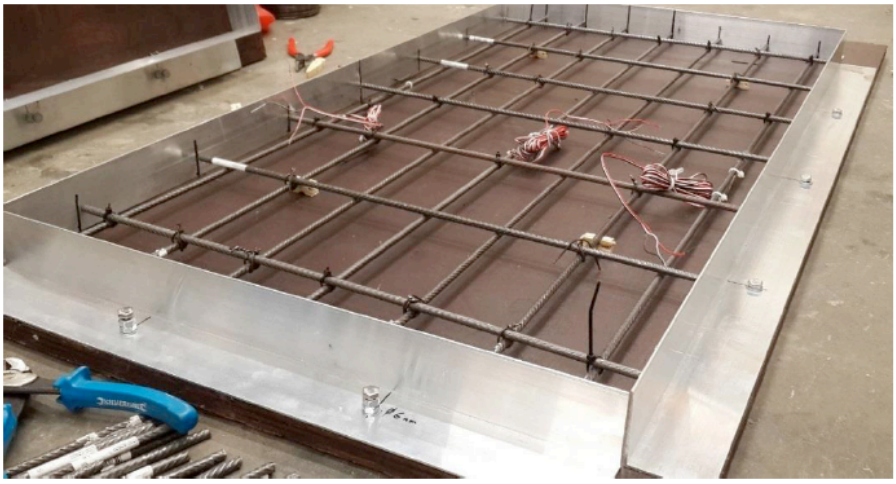

Figure 3: Specifications of the main rebar bottom layer within the samples.

making/curing followed BS EN 12390-2. The mean compressive strength at test is reported per specimen in Table **1**.

2.2.2. Steel Reinforcement

All specimens were detailed with similar main reinforcement, consisting of a two-way mesh of steel bars at the bottom face, as shown in Figures **1** and **3**. The longitudinal reinforcement comprised 6 mm diameter ribbed bars arranged parallel to the slab length at 70 mm spacing, with a 10 mm cover from the bottom fiber, primarily resisting flexural actions. Transverse reinforcement consisted of 6 mm ribbed bars placed orthogonally to the longitudinal bars at 140 mm spacing, intended to control shrinkage and temperature effects.

The mechanical properties of the reinforcement were determined through tensile tests performed on an INSTRON 1341 universal testing machine. Figure **4** presents a typical stress–strain curve obtained from standard tensile testing in accordance with BS EN ISO 6892-1 (2019). The results indicate a yield stress of 460 MPa and an elastic modulus of 185 GPa. Additional details are provided in Table **3**.

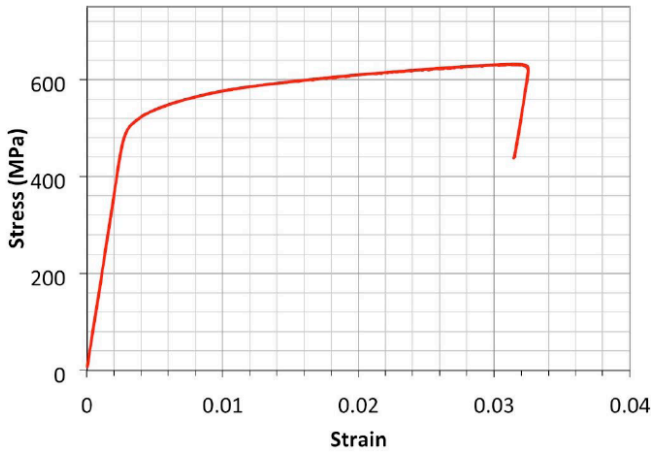

Figure 4: Typical stress-strain behavior observed during standard tensile testing.

2.2.3. CFRP Rods

Pultruded CFRP rods (Ø4 mm), manufactured with T300 carbon fibers in an epoxy matrix (nominal ~60% fiber / 40% resin by volume per manufacturer), were post-installed in epoxy-filled grooves. Mechanical properties were obtained from uniaxial tensile tests on rod coupons (ISO 10406-1 / ASTM D7205). The measured tensile strength and elastic modulus were 1400 MPa and 128 GPa, respectively, implying an

Table 3: Properties of Steel, CFRP Rods, and Epoxy

Property	Steel rebar (ribbed, Ø6)	CFRP rods (T300, Ø4)	Epoxy (Sikadur®-31 CF, 7-day)
Yield strength, fy (MPa)	460	—	—
Tensile strength, fu (MPa)	630	1400	13
Elastic modulus in tension, E (GPa)	185	128	—
Compressive strength (MPa)	—	—	52
Compressive modulus (GPa)	—	—	2.6
Ultimate strain, εu (%)	13 (steel)	≈1.1	—
Surface/finish	Ribbed	Smooth	Thixotropic paste

ultimate strain of ~1.1%. A representative stress–strain response is shown in Figure **5**.

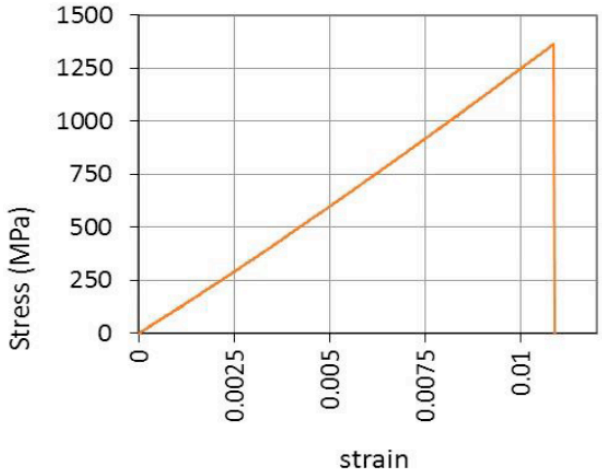

Figure 5: Typical stress-strain relationship observed during the tensile test of the CFRP rod.

2.2.4. Bonding

CFRP rods were bonded into 7 × 7 mm grooves (Figure **1b**) on the top and bottom faces using a two-part structural epoxy (Sikadur®-31 CF). Grooves were cut, edges squared, and cleaned by vacuum, oil-free compressed air, and solvent wipe. Epoxy was applied to all groove faces; rods were inserted with a slight twist to avoid voids, and the grooves were finished flush. Specimens cured at ~20 °C for ≥7 days before testing. Properties of steel, CFRP and epoxy are summarized in Table **3**.

2.3. Construction and Preparation of Specimens

2.3.1. Formwork Preparation

Three rigid molds were built for slabs 1000 × 500 × 50 mm. The soffit used phenolic-faced plywood to obtain a flat finish; all internal faces were sealed. Non-corroding angle cleats were fixed outside the corners to hold squareness; joints were sealed to prevent leakage. A form-release agent was applied uniformly. Molds were levelled (±0.5 mm) before placing reinforcement and spacers. Figure **6** illustrates one of the molds used for fabricating the specimens.

2.3.2. Specimen Fabrication and Curing

Molds were coated with release agent; the reinforcement cage was placed on spacers to achieve the specified nominal bottom cover. Strain gauges were bonded to the main tension bars at mid-span; leads were routed and encapsulated with silicone.

Concrete was placed in shallow lifts and compacted using a small-diameter needle vibrator with short insertions, avoiding contact with steel. The surface was finished to a uniform plane. After finishing, specimens were covered with polythene; at 24 ± 1 h, slabs were demolded and wet-cured under hessian plus plastic sheeting until the test age. Companion cubes were cured in water at 20 ± 2 °C (BS EN 12390-2). Figure **7** depicts the procedures for pouring, compacting the fresh concrete slabs, and preparing concrete samples.

2.3.3. Post-Installed CFRP Rods

Retrofitting of the slabs with CFRP rods using the NSM technique was carried out four weeks after concrete casting. The procedure comprised two main phases.

Phase 1 – Surface preparation: The slab surface was cleaned and leveled, and the locations of the CFRP rods were marked, including their lengths and spacing. Grooves with a 7 × 7 mm cross-section were then cut to receive the rods. The rods had a diameter of

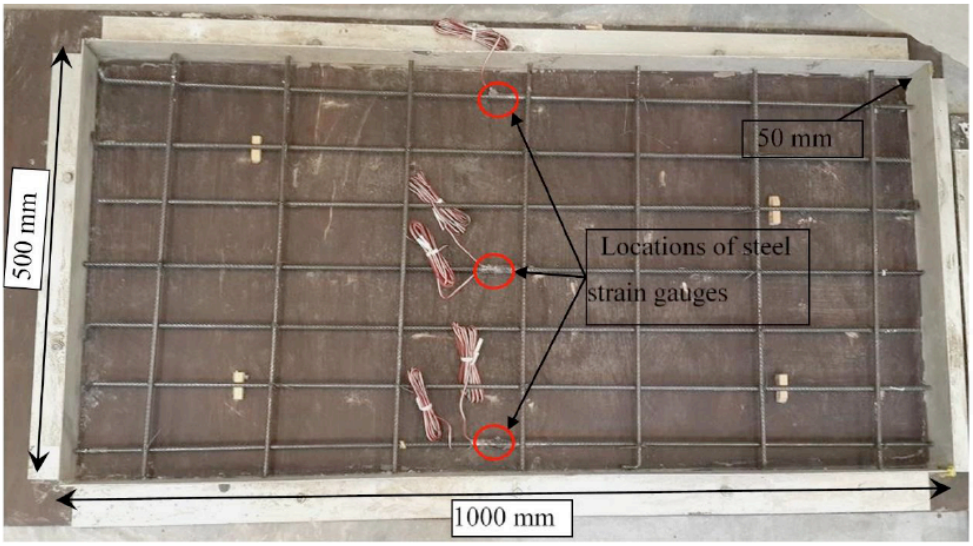

Figure 6: Formwork for concrete slab specimens.

a) Using a manual vibrator to compact the fresh concrete

b) Concrete samples

Figure 7: Concrete casting method including (**a**) pouring and compacting of fresh concrete slabs, and (**b**) preparation of concrete samples.

4 mm, while the epoxy layer was applied with an average thickness of 1.5 mm. A 1500 W wall chaser machine (Draper Expert) was used for cutting.

Phase 2 – Rod installation: The grooves were thoroughly cleaned with compressed air to remove dust and debris generated during cutting. The CFRP rods were then inserted and bonded into the grooves using Sikadur®-31 CF, applied from a cartridge with an application gun. The adhesive was allowed to cure for 24 hours to ensure adequate strength before testing. Figure **8** illustrates the stages involved in post-installing the NSM CFRP rods.

2.4. Instrumentation

Figure **9** shows that the applied load was measured with a Honeywell Sensotec load cell. Mid-span deflection was recorded by an LVDT under the slab centerline. Strain was monitored using Vishay Micro-Measurements C2A-06-125LW-350 rebar gauges (350 Ω) and TML PL-60-11 concrete surface gauges (120 Ω) bonded with M-Bond AE-10. Signals were acquired via a StrainSmart® System 6000 at 1 kHz and later low-pass filtered (10–20 Hz) prior to analysis.

2.4.1. Strain-Gauge Installation

Steel and concrete surfaces were locally flattened/ground (steel: small flat on the rebar; concrete: pad to expose fine aggregate), abraded (180 → 320/400 grit), vacuumed, blown with oil-free air, and wiped with isopropyl alcohol. Gauges were bonded with M-Bond AE-10 under light pressure, leads soldered and strain-relieved, and the assembly over-coated before testing. Electrical checks (bridge balance, insulation >10 MΩ) and shunt calibration were

(a) Preparation of grooves using a wall chaser machine.

(b) Insertion of CFRP rods into the grooves.

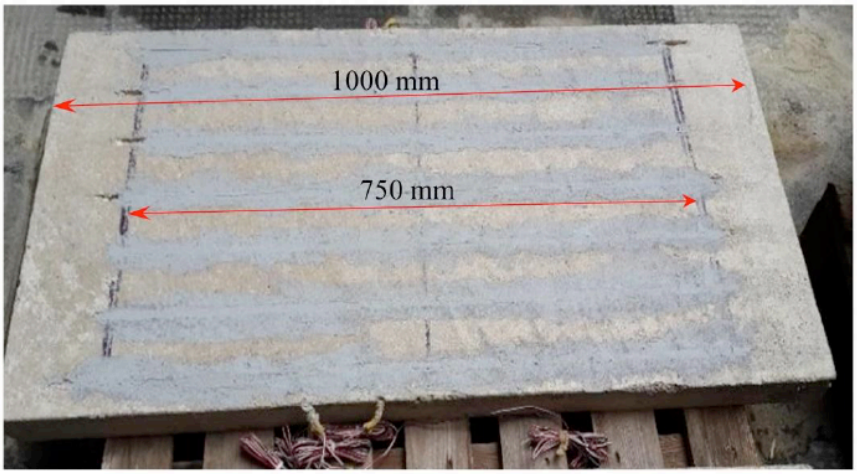

(c) Bonding of CFRP rods inside the grooves using epoxy adhesive.

Figure 8: Construction stages for post-installing the NSM CFRP rods.

performed prior to loading. Figure **10** illustrates photos of the strain gauges installed on both steel and concrete, positioned at the centre of the concrete slab to measure strain in the most critical area.

2.5. Test Setup

Tests were conducted in the Structures Laboratory, University of Bristol. Specimens were simply supported on steel rollers at L = 0.83 m (center-to-center). Load was applied with a manually controlled hydraulic jack acting through an in-line load cell at ~15 kN/min. A whiffletree splits the jack force into four nominally equal point loads arranged symmetrically; outer load spacing and pad sizes are dimensioned in Figure **11**. Neoprene pads were used at load and support interfaces; a small seating preload was applied before data acquisition.

a) StrainSmart® data logger System 6000

b) Load cell

c) LVDT

Figure 9: Sample photos of the measurement devices in experiments.

a) Steel strain gauge **b**) Concrete strain gauge

Figure 10: Sample photos of the strain gauges in experiments.

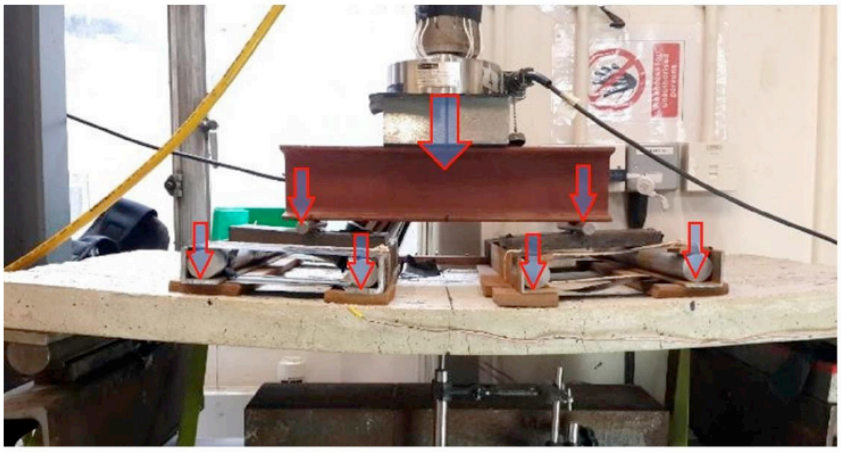

Figure 11: Test setup of four-point load system.

3. EXPERIMENTAL RESULTS

This section reports: (i) load–deflection behavior and ductility, (ii) steel and concrete strain response, (iii) crack development and failure modes, and (iv) energy input and dissipation under cyclic loading. Unless stated, strengthened results are compared with the average of the two controls.

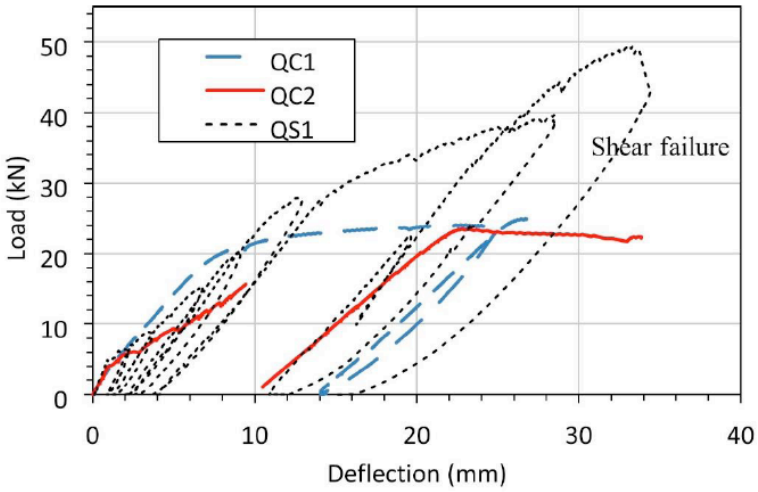

Figure 12: Load-Deflection Behavior of Retrofitted and Conventional Slabs under Quasi-Static Loading.

3.1. Load–Deflection Behavior and Ductility

Ductility was evaluated as the ratio of maximum mid-span displacement to the yield displacement, following the method proposed by Meisami *et al*. (2013). Quasi-static loading was applied incrementally in cycles—two for the conventional slabs and four for the retrofitted slab. During each loading and unloading stage, unloading stiffness was measured to estimate elastic energy absorption.

Figure **12** presents the load–deflection responses of the conventional slabs (QC1 and QC2) and the retrofitted slab (QS1). Table **4** summarizes the key mechanical properties, including yield load (maximum load before significant plastic deformation), load capacity (maximum load before failure), yield deflection, ultimate deflection, ductility factor, dissipated energy, and failure mode. Together, these parameters provide a comprehensive assessment of the slabs' structural performance under quasi-static loading. It should be noted that the second loading stage of slab QC2 was not recorded due to an LVDT malfunction.

The results indicate load capacities of 25.1 kN (QC1), 23.5 kN (QC2), and 49.4 kN (QS1), confirming a significant increase of about 97% for the retrofitted slab. Peak mid-span deflections were 27.3 mm, 34.0 mm, and 34.4 mm for QC1, QC2, and QS1, respectively. The corresponding ductility factors were 3.3, 3.0, and 2.4, showing a reduction of roughly 20% in the strengthened slab compared to the conventional slabs. This decrease was expected due to the addition of 3 Ø4 mm NSM CFRP rods in the tension zone, which limited plastic deformation. However, the inclusion of 7 Ø4 mm NSM CFRP rods on the compression face contributed to maintaining ductility, in line with observations from earlier studies (Ramana *et al*., 2000; Dias *et al*., 2018).

3.2. Crack Pattern and Failure Mode

Figure **13**-**b** shows the crack pattern at the bottom surface of the conventional slabs, dominated by a single major open crack in the tension zone that ultimately led to concrete crushing (Figure **16**-**a**). By contrast, the retrofitted slab (Figure **15**-**b**) exhibited

Table 4: Mechanical Properties and Test Results of the Slabs

Slab	State	Compression strength of concrete (MPa)	Yield load (kN)	Load Capacity (kN)	Yield deflection (mm)	Ultimate deflection (mm)	Ductility	Dissipated energy	Failure mode
QC1	Conventional	41.7	17.4	25.1	6.3	27.3	3.3	424	CC
QC2	Conventional	39.9	13.8	23.5	8.4	34.0	3.0	-	CC
QS1	Strengthened	43.2	18.9	49.4	10.0	34.4	2.4	901	SF
In which, CC denotes concrete crushing, and SF stands for shear failure.									

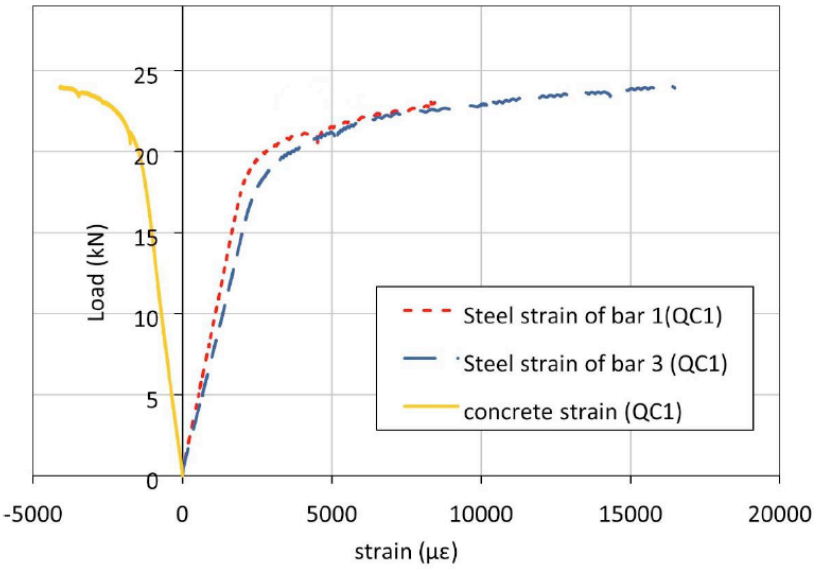

b) Load-strain behavior of conventional slab QC1.

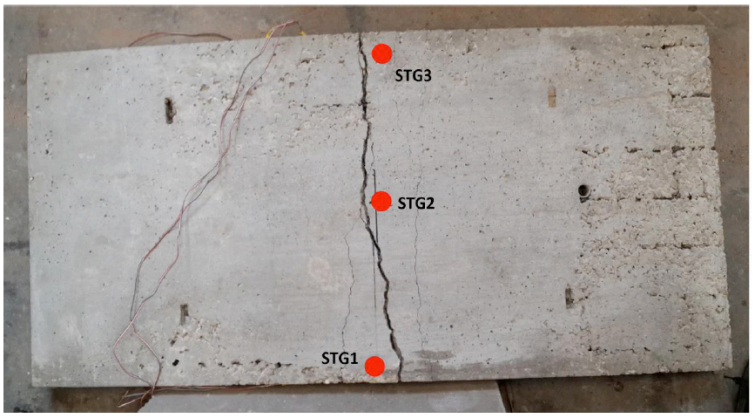

a) Major Tensile Crack in Concrete at Conventional Slab QC1

Figure 13: Load-strain behavior and major tensile crack in conventional slab QC1.

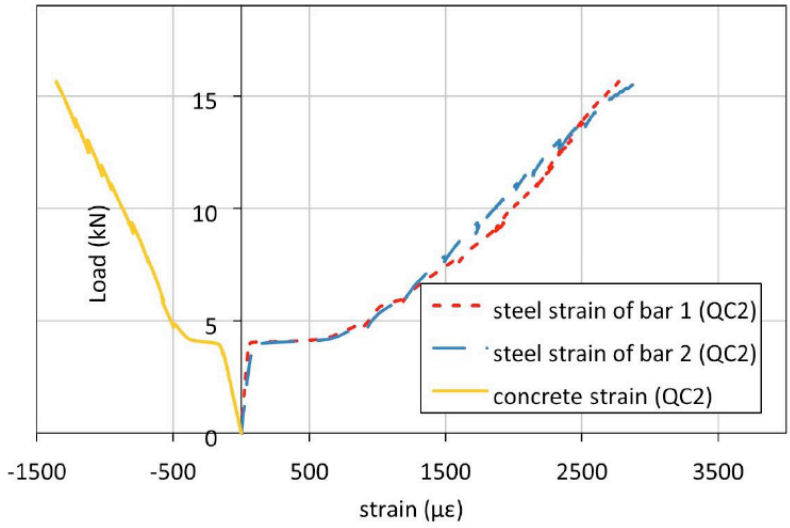

Figure 14: Load-strain behavior of conventional slab (QC2).

multiple fine cracks evenly distributed along the bottom fiber, reflecting improved flexural resistance. However, this enhanced flexural capacity shifted the governing failure mode to shear (Figure **16**-**b**), as the slabs were not provided with shear reinforcement. Similar shear failure was observed from similar tests (Sharaky *et al*. 2023).

Visual observations during and after testing confirmed strong adhesion of the post-installed CFRP rods to the surrounding concrete, despite their near-surface placement. The Sikadur®-31 CF epoxy remained intact and free from visible cracking. These results highlight the robustness of the NSM technique, which mitigates premature debonding—a common weakness in externally bonded (EB) systems, where delamination of composite laminates often triggers early failure (Lee *et al*., 2008; Mukhopadhyaya & Swamy, 2001; Sebastian, 2001).

3.3. Load–Strain Behavior

The load–strain responses of the concrete bottom surface and main reinforcement at mid-span for slabs QC1, QC2, and QS1 are shown in Figures **13**-**a**, **14**, and **15**-**a**, respectively.

For slab QC1 (Figure **13**-**a**), the response remained linear elastic up to an applied load of about 20 kN, after which the strain readings from the concrete bottom surface and strain gauges STG1 and STG3 transitioned into the nonlinear plastic range, leading ultimately to failure.

For slab QC2 (Figure **14**), some setup instability was observed, producing an abrupt strain jump at approximately 4 kN, attributed to tensile cracking at the bottom surface.

For the retrofitted slab QS1 (Figure **15**-**a**), the load–strain curves remained linear elastic until about 26 kN—representing an increase of roughly 30% compared to slab QC1—before entering the nonlinear range.

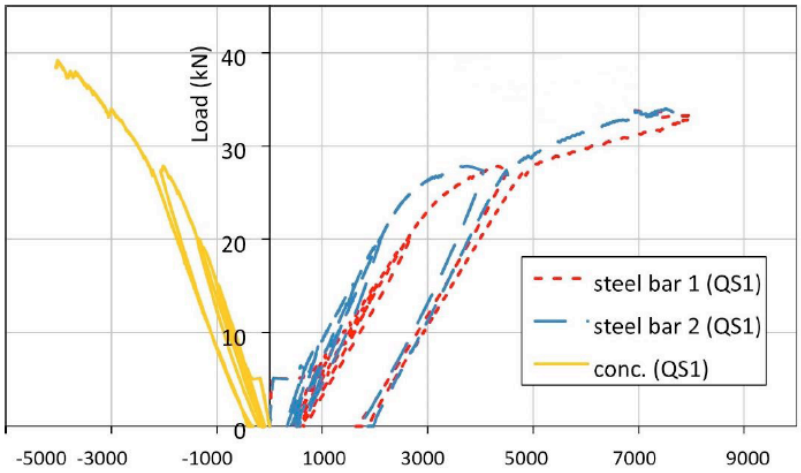

a) Load-strain behavior of retrofitted slab QS1.

b) Evenly distributed tensile cracks at bottom face of slab QS1

Figure 15: Load-strain behavior and tensile crack distribution of retrofitted slab QS1

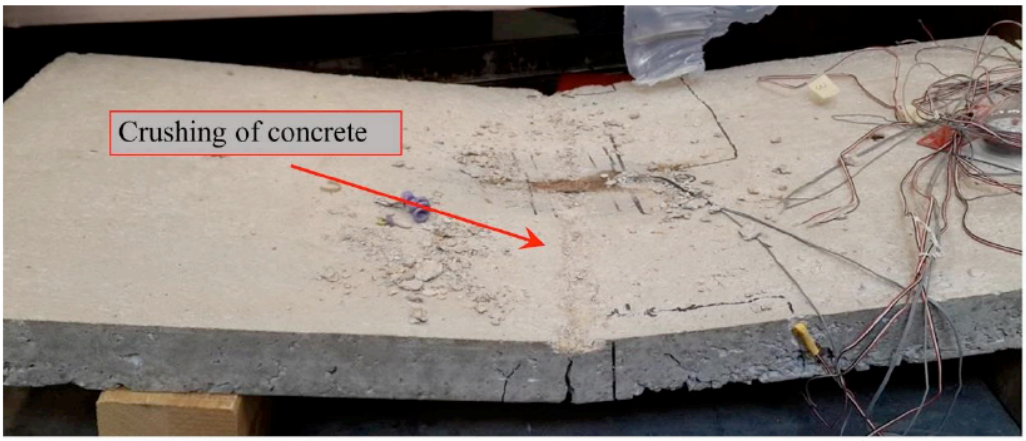

a) Crushing failure mode of slab QC1.

b) Concrete inclined shearing of slab QS1.

Figure 16: Failure Modes of conventional slab QC1and retrofitted slab QS1.

3.4. Energy Input and Dissipation

Let P(Δ) denote the applied load as a function of mid-span deflection. The input energy up to a deflection Δ_{end} is

$$E_{in} = \int_0^{\Delta_{end}} P(\Delta)\, d\Delta$$

Under cyclic loading, the dissipated energy per cycle is given by the enclosed hysteresis loop area,

$$W_{d,i} = \oint_{cycle\ i} P(\Delta)\, d\Delta$$

evaluated numerically using the trapezoidal rule on filtered load–deflection records. The cumulative dissipated energy to failure is then

$$W_{d,cum} = \sum_i W_{d,i}$$

Because the control slabs (QC1 and QC2) were subjected to two load cycles, while the strengthened slab (QS1) underwent four, results are reported in two ways:

1. **Equal-cycle comparison** — based on the first two cycles for all slabs.
2. **Cumulative comparison** — based on all available cycles, acknowledging the difference in cycle counts.

From Table **4**, QS1 exhibited markedly greater energy dissipation. Its cumulative value reached 901 units, representing an increase of approximately **+112% relative to QC1** (424 units). Equal-cycle values are reported separately in the dataset/repository.

4. CONCLUSIONS

This study evaluated thin (50 mm) one-way RC slabs retrofitted with NSM CFRP rods under quasi-static loading. Two slabs were controls; one slab was strengthened with seven Ø4 mm CFRP rods at the bottom (tension) face and three Ø4 mm rods at the top (compression) face.

1) Strength, ductility, energy: The strengthened slab reached ~+103% higher ultimate load than the control mean (49.4 vs 24.3 kN) and ~24% lower ductility (2.4 vs 3.15). Hysteretic dissipation was markedly higher; equal-cycle (1–2) and cumulative values are both reported.

2) Cracking and failure: Controls failed in flexure with top-face crushing; the strengthened slab exhibited denser flexural cracking and a one-way flexure–shear

failure near peak—consistent with raised flexural capacity without increased shear resistance in slabs lacking shear reinforcement.

3) Bond: No visible debonding, cover splitting, or rod pull-out was observed for Ø4 rods in 7×7 mm grooves bonded with Sikadur®-31 CF at the achieved load levels.

4) Implication: NSM CFRP can double flexural capacity of very thin one-way slabs but reduces ductility; designers should check shear (a/d) explicitly and consider complementary shear provisions where needed.

5) Limitations: n = 1 strengthened and n = 2 controls; results should be validated with additional specimens and parameter studies (rod spacing, edge distance, adhesive type/surface finish).

ACKNOWLEDGMENTS

Acknowledgments — The authors thank W. Sebastian, J. Agarwal and J. Macdonald, and the Structures Laboratory technicians at the University of Bristol. This work was supported by the University of Baghdad and the Iraqi Ministry of Higher Education and Scientific Research. The views expressed are those of the authors.

CONFLICT OF INTEREST

The authors declared no potential conflicts of interest with respect to the research, authorship, and/or publication of this article.

REFERENCES

[1] Adriana S. Azevedo, João P. Firmo, João R. Correia, 2024. Three-dimensional finite element modelling of the fire response of passive and prestressed near-surface mounted (NSM)-CFRP-strengthened reinforced concrete slab strips. Composite Structures, Volume 331, 117872. https://doi.org/10.1016/j.compstruct.2023.117872

[2] Adriana S. Azevedo, João P. Firmo, João R. Correia, Reza M. Firouz, Joaquim A.O. Barros, 2023. Fire behavior of reinforced concrete slab strips strengthened with prestressed NSM-CFRP laminates. Engineering Structures, Volume 297, 116982. https://doi.org/10.1016/j.engstruct.2023.116982

[3] Alkhrdaji, T. & Nanni, A. Surface bonded FRP reinforcement for strengthening/repair of structural reinforced concrete. Proc., ICRI-NRCC Workshop, Baltimore, MD (USA), Oct 1999. 19.

[4] Aljidda, O., El Refai, A., Alnahhal, W., Experimental and analytical investigation on the use of NSM–BFRP and NSM–GFRP bars in strengthening corrosion–damaged RC slabs, Composite Structures, Volume 322, 2023, 117428. https://doi.org/10.1016/j.compstruct.2023.117428

[5] Asplund, S. Strengthening bridge slabs with grouted reinforcement. Journal Proceedings, 1949. 397-406.

[6] Barros, J. A., Ferreira, D. R., Fortes, A. S. & Dias, S. J. 2006. Assessing the effectiveness of embedding CFRP laminates in the near surface for structural strengthening. Construction and Building Materials, 20, 478-491. https://doi.org/10.1016/j.conbuildmat.2005.01.030

[7] Berger, J., Heffernan, P. & Wight, R. 2008. Blast testing of CFRP and SRP strengthened RC columns. Structures Under Shock and Impact, 98, 95-104. https://doi.org/10.2495/SU080101

[8] BS 1881-124. 2021. Testing Concrete - Methods for analysis of hardened concrete, British Standard Institution, London, UK.

[9] BS EN 12390-3. 2019. Testing hardened concrete - Compressive strength of test specimens. British Standard Institution, London, UK.

[10] BS EN ISO 6892-1. 2019. Metallic materials. Tensile testing - Method of test at room temperature. British Standard Institution, London, UK.

[11] De Lorenzis, L. & Teng, J. 2007. Near-surface mounted FRP reinforcement: An emerging technique for strengthening structures. Composites Part B: Engineering, 38, 119-143. https://doi.org/10.1016/j.compositesb.2006.08.003

[12] Dias, S., Barros, J. & Janwaen, W. 2018. Behavior of Rc Beams Flexurally Strengthened with NSM CFRP Laminates. Composite Structures, 201, 363-376. https://doi.org/10.1016/j.compstruct.2018.05.126

[13] Eurocode 2. 2004. Eurocode 2: Design of concrete structures, Part 1-1: General rules and rules for buildings. BS EN 1992-1-1, London. UK.

[14] Frangou, M., Pilakoutas, K. & Dritsos, S. 1995. Structural repair/strengthening of RC columns. Construction and building materials, 9, 259266. https://doi.org/10.1016/0950-0618(95)00013-6

[15] Ha, J. H., Yi, N. H., Choi, J. K. & Kim, J. H. J. 2011. Experimental study on hybrid CFRP-PU strengthening effect on RC panels under blast loading. Composite Structures, 93, 2070-2082. https://doi.org/10.1016/j.compstruct.2011.02.014

[16] Hosseini, M. M., Dias, S. J. & Barros, J. A. 2014. Effectiveness of prestressed NSM CFRP laminates for the flexural strengthening of RC slabs. Composite Structures, 111, 249-258. https://doi.org/10.1016/j.compstruct.2013.12.018

[17] Kim, JHJ, Yi, NH, Kim, SB, Choi, JK & Park, JC 2009, 'Experiment study on blast loading response of FRP-retrofitted RC slab structures', Paper presented at 2nd Asia-Pacific Conference on FRP in Structures, APFIS 2009, Seoul, Korea, Republic of, 09/12/9 - 09/12/11 pp. 533-538.

[18] Lee, S. K., Chen, Z., Ng, M., Tang, J., Wan, L., Liu, M. & Lee, L. 2008. Evaluation of CFRP, GFRP and BFRP Material Systems for the Strengthening of RC Slabs. Journal of reinforced plastics and composites.

[19] Meisami, M. H., Mostofinejad, D. & Nakamura, H. 2013. Punching shear strengthening of two-way flat slabs using CFRP rods. Composite Structures, 99, 112-122. https://doi.org/10.1016/j.compstruct.2012.11.028

[20] Mosallam, A. S. & Mosalam, K. M. 2003. Strengthening of two-way concrete slabs with FRP composite laminates. Construction and Building Materials, 17, 43-54. https://doi.org/10.1016/S0950-0618(02)00092-2

[21] Mukhopadhyaya, P. & Swamy, N. 2001. Interface shear stress: a new design criterion for plate debonding. Journal of Composites for Construction, 5, 35-43. https://doi.org/10.1061/(ASCE)1090-0268(2001)5:1(35)

[22] Muszynski, L. C. & Purcell, M. R. 2003. Composite reinforcement to strengthen existing concrete structures against air blast. Journal of Composites for Construction, 7, 93-97. https://doi.org/10.1061/(ASCE)1090-0268(2003)7:2(93)

[23] Ramana, V.P.V., Kant, T., Morton, S., Dutta, P., Mukherjee, A. & Desai, Y. 2000. Behavior of CFRPC strengthened reinforced concrete beams with varying degrees of strengthening. Composites Part B: Engineering, 31, 461-470. https://doi.org/10.1016/S1359-8368(00)00022-6

[24] Razaqpur, A. G., Contestabile, E. & Tolba, A. 2009. Experimental study of the strength and deformations of carbon fiber reinforced polymer (CFRP) retrofitted reinforced concrete slabs under blast load. Canadian Journal of Civil

Engineering, 36, 1366-1377.
https://doi.org/10.1139/L09-002

[25] Sastranegara, A., Adachi, T. & Yamaji, A. 2005. Improvement of energy absorption of impacted column due to transverse impact. International journal of impact engineering, 31, 483-496.
https://doi.org/10.1016/j.ijimpeng.2003.12.009

[26] Sebastian, W. M. 2001. Significance of midspan debonding failure in FRP-plated concrete beams. Journal of Structural Engineering, 127, 792-798.
https://doi.org/10.1061/(ASCE)0733-9445(2001)127:7(792)

[27] Silva, P. F. & Lu, B. 2007. Improving the blast resistance capacity of RC slabs with innovative composite materials. Composites Part B: Engineering, 38, 523-534.
https://doi.org/10.1016/j.compositesb.2006.06.015

[28] Sharaky, I.A., Elamary, A.S., Alharthi, Y.M., Experimental and numerical investigation on the flexural performance of RC slabs strengthened with EB/NSM CFRP reinforcement and bonded reinforced HSC layers, Engineering Structures, Volume 289, 2023, 116338,
https://doi.org/10.1016/j.engstruct.2023.116338

[29] Täljsten, B., Carolin, A. & Nordin, H. 2003. Concrete structures strengthened with near surface mounted reinforcement of CFRP. Advances in structural engineering, 6, 201-213.
https://doi.org/10.1260/136943303322419223

[30] Tabatabaei, Z. S., Volz, J. S., Gliha, B. P. & Keener, D. I. 2012. Development of long carbon fiber-reinforced concrete for dynamic strengthening. Journal of Materials in Civil Engineering, 25, 1446-1455.
https://doi.org/10.1061/(ASCE)MT.1943-5533.0000692

[31] Wang, S. Y. & Wang, Z. Y. 2013. Mechanism of improving ductility of high strength concrete T-section beam confined by CFRP sheet subjected to flexural loading. Journal of Central South University, 20, 246-255.
https://doi.org/10.1007/s11771-013-1482-2

[32] Wu, C., Oehlers, D. J., Wachl, J., Glynn, C., Spencer, A., Merrigan, M. & Day, I. 2007. Blast testing of RC slabs retrofitted with NSM CFRP plates. Advances in Structural Engineering, 10, 397-414.
https://doi.org/10.1260/136943307783239372

https://doi.org/10.12974/2311-8717.2025.13.05